JOURNAL OF MATERIALS SCIENCE 35 (2000) 3561–3571

Surface structure and surface-spin induced magnetic properties and spin-glass transition in nanometer Co-granules of FCC crystal structure

S. RAM
Materials Science Centre, Indian Institute of Technology, Kharagpur-721302, India
E-mail: sram@matsc.iitkgp.ernet.in

Separated Co-granules, of an average diameter as small as $D = 2.0$ nm, of FCC crystal structure have been synthesized by co-reducing Co^{2+} cations dispersed in a liquid. They exhibit an enhanced saturation magnetization σ_s by as much as ~34% with a more than an order of enhanced magnitude for the effective anisotropy constant K_{eff} over the bulk values at 4.2 K. An irreversibility in the ZFC-FC (zero field cooled-field cooled) thermomagnetograms occurs at temperatures $T \leq T_B$, where T_B is their blocking temperature. The ZFC thermomagnetogram peaks at T_B according to their K_{eff} and volume V. $T_B = 152$ K has been found for $D = 10$ nm granules in an applied magnetic field of $H = 1$ kA/m. The sample, which is superparamagnetic (coercivity $H_c = 0$) in nature at $T \geq T_B$, develops H_c at $T < T_B$ with a unique dependence on temperature, $H_c(T) = H_c(0)[1 - T/T_B]^{1/2}$, with $H_c(0) = 40.0$ kA/m. The results are discussed with a two-phase model structure of granules. In this model, the grain-surface atoms have a modified magnetic structure of the core atoms. An inter-coupling between the magnetic spins in the two regions occurs in a ferromagnetic or antiferromagnetic manner according to their interface that mediates their exchange interactions through it. The studies of σ, K_{eff}, or H_c as a function of temperature (4.2 to 380 K) and/or size D (2 to 20 nm) demonstrate their strong correlation with the dynamics of the surface spins (DSS). An enhanced surface anisotropy with large total interface-energy in small granules governs the DSS. An average value of the surface anisotropy constant $K_s = 2.28$ mJ/m^2 is determined by a linear plot of K_{eff} with D^{-1} at $D \leq 2.9$ nm. Larger granules follow a modified $K_{eff} - D^{-1}$ plot with an order of smaller K_s-value. The surface spins form a surface-spin-glass, which undergoes a magnetic transition to a spin-frozen state at a critical temperature $T_F = 71$ K. The T_F evolves following the well-known de Almeida-Thouless line, $\delta T_F \propto H^{2/3}$, at $H \leq 42$ kA/m. © *2000 Kluwer Academic Publishers*

1. Introduction

Small magnetic particles of size of a nanometer scale are a subject of intense research in these days owing to their unique magnetic properties which make them very appealing from both the theoretical and the technological points of view [1–10]. They are widely used as permanent magnets [1, 6, 11], information storage systems [3, 12, 13], magnetic toner in xerography [14], ferrofluids [15], contrast agents in magnetic resonance imaging [12, 14], magnetooptic or magnetoresistance devices [8, 16], and chemical catalysts [17, 18]. Below a critical size D_c, i.e. ~20 nm for cobalt or iron [1], they become single domain in nature in contrast with the usual multidomain structure of the bulk material and exhibit unique phenomena of quantum size effects [19], superparamagnetism [14, 20], quantum tunneling of magnetization [21], and unusually large surface (H_s) and magnetocrystalline (H_a) anisotropies [3, 5].

A large fraction of 20 to 60% atoms in such small particles are the surface atoms. These surface atoms have a modified electronic or magnetic structure of the core atoms [17, 18] that leads to a significant change in their H_a and H_s anisotropies and magnetic moment μ_n. It is well established from first principles self-consistent local spin-density calculations that the magnetic moment in the topmost layer(s) in magnetic 3d-transuition metals is generally enhanced as much as 50% over the bulk value [8, 22]. This is ascribed to the reduction in coordination number and coordination symmetry of the surface atoms. It causes the bands narrow and hence, in general, enhances the paramagnetic density at the Fermi level E_F [22]. Considerably modified magnetic hyperfine fields of the core atoms have been shown in the surface atoms [23]. Chen *et al.* observed that as small Co-granules as 1.8 nm have ~30% increased μ_n over the bulk value [5]. Recently, there has been a considerable work on atomic clusters [24–26]. The cluster of iron, cobalt, or nickel assumes a similar increase in μ_n as the number of atoms in it falls from several hundred to a few tens of atoms. Rhodium, which is paramagnetic

in the bulk, becomes ferromagnetic in the clusters of 30 atoms or less [25].

Obviously, the surface structure and surface spin magnetism in so small crystallites are primarily governed by their enhanced surface-spin-density (SSD) by the enhanced surface or total surface-energy Ω. Ω, which controls their morphology, attenuates the distribution of the surface spins and their exchange interactions through the core spins. In process of magnetization (which occurs through H_a and H_s) in an assembly of randomly oriented single domain particles, the surface magnetism controls the dynamics of the surface spins as well as of the particle as a whole according to its size. The direction of the magnetization fluctuates spontaneously (superparamagnetic relaxation) with a relaxation time $\tau = \tau_0 \exp(\Delta E_a/kT)$, where kT is the Boltzmann's constant k times the temperature T [23]. τ_0 is of the order of 0.1–0.0001 ns and ΔE_a is the anisotropy energy barrier, which can be expressed as the product of an effective anisotropy energy constant K_{eff} and the particle volume V. A particle exhibits a coercivity H_c as long as the ΔE_a dominates over its thermal energy kT. In the classical theory of magnetism [14, 27], $H_c = 0$ for the superparamagnetic particles with $kT \geq \Delta E_a$. The critical temperature at which their metastable hysteresis response disappears is called the blocking temperature T_B [27].

As it is the bulk value of H_a for cobalt (588.9 kA/m) or other magnetic 3d-transition metals is too small [27] to maintain a simple spin configuration (of ideal single magnetic domain particles) within a nanometer scale magnet. It causes the analysis of the experimental data to be difficult. If it becomes possible to prepare so small particles of a significantly improved H_a, their simple spin structures, currently viewed as a two-level system [5, 11, 18, 25], will promote our general understanding of their intrinsic magnetic behaviors. Fortunately, it is achieved with Co-granules of the nanometer size with an order of improved magnitude of H_a of the bulk value [5].

Since the pioneering work of Neel [28], the underlying mechanisms of magnetism, magnetization reversal, and H_c in single domain particles have been much discussed. The knowledge of these processes is very basic in magnetism and is based on the Stoner-Wohlfarth model [29] or numerical micromagnetic calculations [9, 22]. These processes have essential implications in magnetic switching and magnetic recording applications [12, 13]. The rapidly increasing growth of technology of high-energy-density magnetic storage poses the question of how far the reduction of volume-to-surface ratio can continue without inducing new sources of information errors.

In spite of the extensive studies of the magnetic and other macroscopic properties of bulk cobalt, very little information is available about the microscopic structure, surface magnetism, and dynamics of the surface spins, and their relation to the magnetic properties in small particles of the nanometer size [5, 8, 9, 14, 22, 30–32]. This is important to develop a clear understanding of the bulk to atomic transition. A major problem in this effort has been the synthesis of a single phase sample of separated granules of a high SSD of the nanometer size. In this investigation, we successfully synthesized such granules of pure FCC cobalt by a chemical reduction of highly dispersed Co^{2+} cations in a liquid. The liquid medium provides a strict control of their size and morphology through its concentration and/or pH.

In this article, we report on their saturation magnetization σ_s, H_c, and uniaxial or surface magnetic anisotropies. The samples in shape of thin platelets of selected 2 to 20 nm diameters were studied at selected temperatures between 380 and 4.2 K by characterizing the surface and/or temperature dependence of these magnetic properties. The results are discussed in correlation with the magnetism and dynamics of the surface magnetic spins which have an inherent relation with the surface structure, size, and morphology in separated granules. The surface spins undergo a magnetic transition to a frozen surface-spin-glass (SSG) state at $T_F = 71$ K if measured in a low magnetic field H as 0.8 to 42 kA/m. Their dynamics is established by the H dependence of T_F.

2. Experimental details

2.1. Synthesis of the Co-granules

The Co-granules were synthesized by a controlled co-reduction of Co^{2+} cations dispersed in a dilute DDAB/toluene solution. Here, DDAB (didodecyldimethyl ammonium bromide), which is an established cationic surfactant [5], traps the reagent in empty micelles of it and forms a transparent solution. It helps the formation of stable Co-granules by preventing their surface oxidation. The process is described as follows.

The Co^{2+} cations ($CoCl_2.6H_2O$) were dissolved in a 10 wt % DDAB solution in toluene at a predetermined concentration of the order of $\sim 10^{-2}$ M. It forms a blue transparent solution. Then argon is bubbled through it (solution A). A highly concentrated ~5 M aqueous solution of $NaBH_4$ (reducing agent) is made and argon is also bubbled through it (solution B). To reduce A into Co-granules, solution B is added drop by drop to it by stirring the mixture. The whole reaction is carried out in an inert argon atmosphere. A highly exothermic reaction occurs between A and B and results in black slurries of reduced Co^{2+} into the Co-granules of a nanometer size. Average temperature of the solution is controlled at ~273 K with an ice bath with NaCl impurities. Otherwise, that unwantedly raises up as high as its boiling point and reoxidizes the sample.

The slurries of the Co granules are filtered, carefully washed in deionized water and toluene, and then immediately dried in vacuum or N_2 gas at room temperature. A thermal annealing at ~500 K in N_2 gas in a subsequent step causes a stable grain-surface passivation/hardening that supports an improved stability of the sample. The sample was stored in an inert gas or hydrocarbon liquid as toluene all the times. It was taken out only for the measurements.

2.2. Measurements of microstructure and magnetic properties

The formation of the Co-granules and their size/ morphology were analyzed with their X-ray diffractogram

TABLE I Morphology and lattice parameters of small granules of FCC allotrope of cobalt metal obtained from the chemical-reduction of the metal cations

Sample[a]	Morphology[b]	a (nm)[a]	V (10^{-3}nm^3)[a]	A (nm^2)[a]
Amorphous	Platelet	—	—	—
FCC Bulk	Platelet	0.3545[c]	44.6	0.754 (16.91)
FCC nanocrystalline				
$D \sim 2.0$ nm	Spherical	0.3577	45.8	0.768 (16.77)
$D \sim 10$ nm	Platelet	0.3535	44.2	0.750 (16.97)
$D \sim 20$ nm	Platelet	0.3525	43.8	0.746 (17.02)
HCP Bulk	Platelet	$a = 0.2507$[c] $c = 0.4070$[c]	66.5	0.939 (14.12)

[a]The structure and lattice parameters, i.e. lattice axis a, volume V, and surface area A, of the sample are analyzed from its x-ray diffractogram. The Figures given in the parentheses refer to the value of A per unit volume of the lattice.
[b]The morphology of the granules is determined from the scanning/transmission electron micrographs.
[c]The lattice parameters are reported for the standard FCC and HCP cobalt from Ref. 39.

and transmission electron micrograph (TEM). X-ray diffractogram was recorded with an x-ray diffractometer by exciting the sample with a filtered CuK_α radiation of wavelength $\lambda = 0.15406$ nm. All the peaks observed in it belong to a single FCC crystal structure of a pure cobalt. We carefully studied several samples and all have shown the same diffractogram. The positions of the peaks were used to calculate the lattice parameters which are given in Table I. The half-bandwidths $\Delta 2\theta_{1/2}$ in the peaks are in accordance with the crystallite size determined independently by the TEM. *In situ* analysis of the compositional maps with an electron microprobe analyzer confirmed a better purity of the sample than 98.5%. No other elemental impurities, except 1–2 at % chemi-absorbed oxygen atoms at grain-surfaces, were found in a detectable amount of ∼0.1 at %.

The magnetic properties were measured of 0.1 to 0.2 g sample, encapsulated in a plastic capsule, at selected temperatures between 4.2 and 380 K with a vibrating sample magnetometer using a magnetic field to ∼6.5 MA/m. A low temperature cryostat, with liquid helium as coolant, was used in conjunction with the magnetometer to perform the measurements at temperatures as low as 4.2 K. The magnetometer was calibrated to give the results in SI units using a standard sample of pure iron metal of $\sigma_s = 217.5$ Am^2/kg at 295 K. Other details are described earlier [2, 6, 10].

3. Results and discussion

3.1. Microstructure and X-ray diffraction analysis

Fig. 1 shows a typical TEM micrograph of a nanocrystalline sample of Co-granules obtained by a co-reduction from Co^{2+} cations as described above. The granules are in shape of well-separated thin platelets of an average diameter $D \sim 10$ nm, volume $V = A\delta \equiv 150$ nm^3, and aspect ratio $D/\delta \sim 5$, with $A \sim 75$ nm^2 the surface area for one of the two flat faces. A similar microstructure of separated Co-granules of nanometer size is not so easy to fabricate by other methods of a pure mechanical attrition or a thermomechanical attrition [30, 33], or a gas condensation process [1, 3, 34]. A mechanical attrition of a ductile metal as cobalt hardly reduces its size below a micrometer scale. On attrition small particles rather expand in thin sheets by deformation and reorganization of their structure at atomic scale [30, 33].

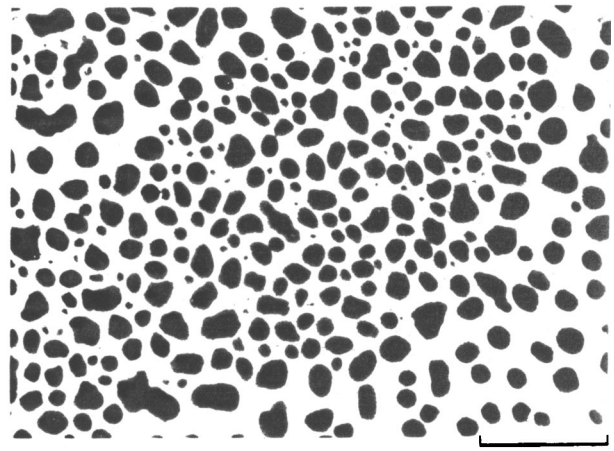

Figure 1 Transmission electron micrograph of the Co-granules of an average 10 nm diameter. The scale bar refers to 50 nm.

The crystalline structure of the sample or its size/morphology solely depends on the experimental conditions of its preparation. The reduction of an extremely dilute (∼10^{-3} M) Co^{2+}-solution thus results in an amorphous Co sample characterized with a broad x-ray diffraction halo (Fig. 2a), with $\Delta 2\theta_{1/2} \sim 7.5^\circ$, at $2\theta = 43.8^\circ$ or scattering vector $k = 5.7$ nm^{-1}, which is defined by $k = 4\pi \sin\theta/\lambda$, with λ the wavelength of the radiation used to measure it [35–37]. A recrystallization of it into the FCC cobalt with a well-defined x-ray diffractogram (Fig. 2b or c) of three characteristic peaks in reflections from (111), (200) and (220) lattice planes occurs on annealing it at 800 K in H_2 gas. This FCC structure is stable over a wide range 0–1023 K of temperature. Note that the most stable allotrope of pure cobalt, as prepared by other methods [1, 38], is the HCP cobalt and it undergoes a martensite transformation to FCC structure around 700 K [38].

The FCC Co-granules of size as small as $D \sim 2.0$ nm have lattice volume $V = 0.3577$ nm^3, which is ∼0.9% lager than the bulk value reported by other methods [38, 39]. This excess volume has regularly decreased to $V = 0.3525$ nm^3, i.e. below the $V = 0.3545$ nm^3 bulk value (Table I), on increasing their size to $D \sim 20$ nm by annealing the sample at 1023 K for 30 min in H_2

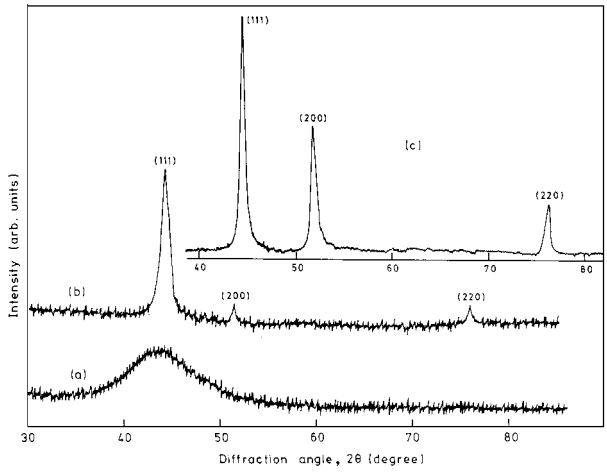

Figure 2 X-ray diffractograms of (a) amorphous and (b) or (c) nanocrystalline Co-metal powders. Samples (b) and (c) are deduced by annealing sample (a) for 30 min at 800 K and 1023 K, respectively, in a pure H_2 gas.

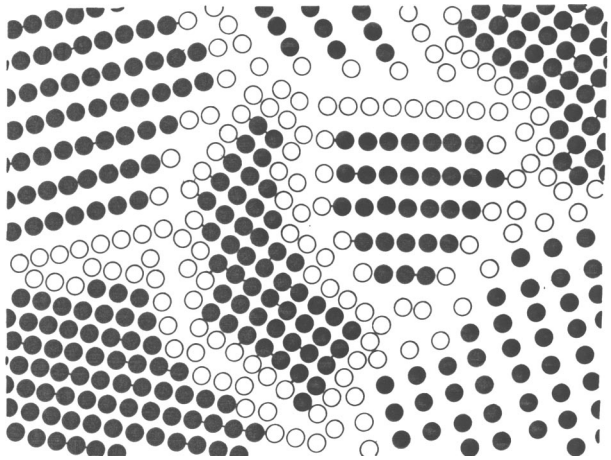

Figure 3 A model distribution of atoms in a nanocrystalline metal. The atoms forming the core and surface of the grains are shown by the filled and open circles. The surface atoms have a slightly off positions of the core atoms [after Gleiter in ref. 17].

gas. It is clearly reflected in shift of the x-ray diffraction peaks in Fig. 2c, in respect to those in Fig. 2b, towards the lower 2θ-values with reduced $\Delta 2\theta_{1/2}$ values according to D. An average value of $D = 8.5$ nm, against the observed value of 10 nm from the TEM (Fig. 1), is calculated using the $\Delta 2\theta_{1/2}$ values in the Debye-Scherrer relation [40]. Its small difference with the observed value indicates a significant lattice strain in the separated Co-granules. That adds ∼15% value in the total $\Delta 2\theta_{1/2}$. It supports their enhanced lattice volume, as much as 1.5%, as mentioned above.

In 2 to 20 nm granules of FCC cobalt, a significant 60 to 20% fraction of the total atoms forms their surface with an essentially modified distribution of the core atoms [17, 18]. A model distribution of atoms, as proposed by Gleiter [17], is shown in Fig. 3. According to it, the core atoms (the filled circles) occupy their regular crystallographic interstitial sites while the atoms at the surface (the open circles) assume their slightly off interstitial positions in order to attain a thermodynamically stable equilibrium configuration of the system of internal-energy ε_{nc}. The grain surface, which has a lower co-ordination number and a lower symmetry of atoms than the core, assumes a lower atomic density on a larger interatomic distance according to the thermodynamics [34]. It results in two structural components; (i) the crystalline component (CC) of the core atoms and (ii) the intercrystalline component (IC) of the surface atoms, in such small grains. The IC includes the boundaries between the crystallites.

The atoms in CC share their electronic charges by regular co-ordinations with the neighbors so that there is no unbalance electronic charge, i.e. $\sum_i \Delta q_i = 0$. This is not true with the IC atoms in their incomplete co-ordinations n_i with the neighbors. The presumed gradient of Δq_i or Δn_i in distributions of atoms in the two regions in an isolated grain causes a redistribution of prominently IC atoms in ε'_{nc} surface-energy states above the equilibrium bulk energy-state ε_0 or ε_{nc}. In view of thermodynamics [10, 27, 34], it involves a modified set of state functions of internal energy ε, volume V, enthalpy H, or entropy S of usually enhanced values of their equilibrium bulk values. They ascribe modified magnetic structure and magnetic properties in small granules as discussed below.

3.2. Magnetic properties

3.2.1. Surface magnetization

The Co granules of average $D \sim 10$ nm diameter have saturation magnetization $\sigma_s = 173$ Am^2/kg (163 Am^2/kg at RT) at 4.2 K. This value, which is ∼4.2% larger than the bulk $\sigma_s = 166.1$ Am^2/kg value [27, 41], is further enhanced to $\sigma_s = 178$ Am^2/kg on annealing the sample at 1023 K in H_2 gas. The annealing reduces grain-surface-passivation (GSP), if any, formed by surface oxidation of the granules during the synthesis process. As the GSP is less magnetic in comparison to the strong ferromagnetic core [4], its reduction results in an increase in the total σ_s value. Childress and Chien reported a similar enhanced $\sigma_s(t) = 175$ Am^2/kg (at 4.2 K) for FCC cobalt by extrapolation of $\sigma_s(t)$ with $x \to 1$ in Co_xCu_{1-x} intermetallics, which maintains a single phase FCC structure up to $x = 0.8$ [42]. The FCC structure also in this series could be fabricated only by a nonequilibrium method of magnetron sputtering [42].

A change in the total $\sigma_s(t)$ with a change in GSP in this example can be described with a simple relation,

$$\sigma_s(t) = \frac{\sigma_s(c)V_c\rho_c \pm \sigma_s(s)V_s\rho_s}{(V_c + V_s)\rho_t}, \qquad (1)$$

or,

$$\sigma_s(t) = \frac{\sigma_s(c)V_c \pm \sigma_s(s)V_s}{(V_c + V_s)}, \quad \text{if} \quad \rho_s \sim \rho_c \sim \rho_t, \quad (2)$$

where, $\sigma_s(c)$ is the σ_s value for the core of volume V_c and density ρ_c while $\sigma_s(s)$ is the σ_s value for the GSP of volume V_s and density ρ_s in a Co-granule of the total volume $V = V_c + V_s$ and average density ρ_t. If the magnetic moment of the GSP is assumed to be negligibly small in comparison to that for the core, i.e.,

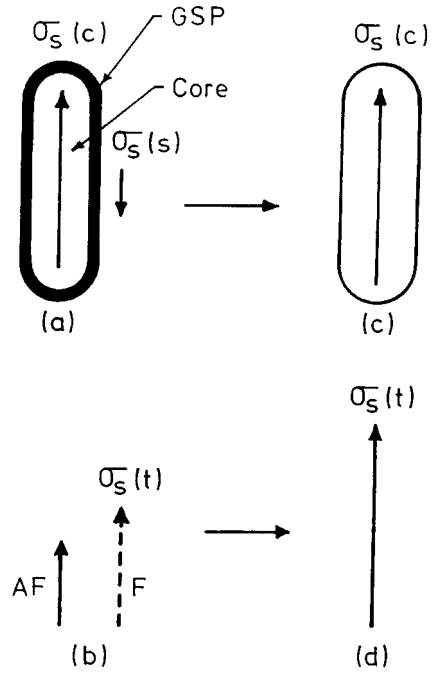

Figure 4 A model distribution of magnetizations in the core $\sigma_s(c)$ and grain-surface-passivation (GSP) $\sigma_s(s)$ of equal volumes in a small Co-granule with $\sigma_s(c)/\sigma_s(s) = 0.2$. Their resultant $\sigma_s(t) = 0.5\{\sigma_s(c) - \sigma_s(s)\}$ presents a lower value in an antiferromagnetic (AF) coupling over a ferromagnetic (F) coupling, shown by the arrow with the dash, in (b). (c) A removal of GSP results in a more pronounced increase in the $\sigma_s(t)$ in (d) in the AF coupling.

$\sigma_s(c) \ll \sigma_s(s)$, this relation further simplifies to

$$\sigma_s(t) = \frac{V_c}{(V_c + V_s)}\sigma_s(c) \qquad (3)$$

It yields a fractional volume of GSP as small as $V_s = 2.8\%$ for $D \sim 10$ nm granules, using the observed values of $\sigma_s(t) = 173$ Am^2/kg and $\sigma_s(c) = 178$ Am^2/kg for the sample before and after annealing it in H_2 gas to remove the GSP film. This small value of V_s reveals an extremely small thickness $\varepsilon \sim 0.02$ nm, i.e. smaller than expected in a monatomic layer, for it, with $\sigma_s(s) \sim 0$, in this sample of thin platelets of $V = A\delta \cong 150$ nm^3, width $\delta \sim 2$ nm, and surface area (for one of the flat surfaces) $A = 75$ nm^2 (Fig. 1). In the fact, it can never be a thinner than a monatomic layer. A over simplification of its $\sigma_s(s) \sim 0$ led to this difference.

In fact, the $\sigma_s(s)$ in GSP has a significant value. It is coupled with $\sigma_s(c)$ in the core in a ferromagnetic (F) or antiferromagnetic (AF) fashion according to exchange interactions (EXI) between the magnetic spins in the two reigns. The EXI in this case depends on the H_a or H_s anisotropies, the relative magnitude of $\sigma_s(s)$, and the thickness of the GSP film ε. The distribution of the spins in the GSP and GSP-core interface designs according to ε and it ultimately controls their dynamics and exchange coupling with the spins in the core. As demonstrated in Fig. 4, in either case of F or AF distribution of the spins, a decrease in ε leads to an increase in the total $\sigma_s(t)$ value. The effect is less pronounced in the F distribution in the two regions, in consistent with the experimental observation, which reveals only a small 2.8% increase in $\sigma_t(s)$ on reducing the GSP film

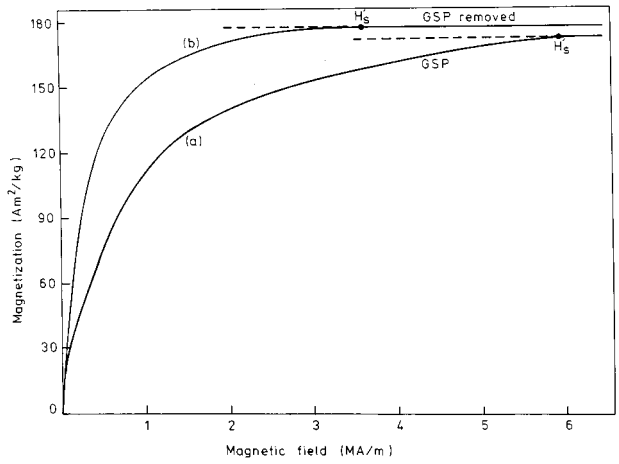

Figure 5 σ vs H magnetization in Co-granules, $D = 10$ nm; (a) before, and (b) after hating the sample at 700 K for 30 min in H_2 gas to remove the GSP. The σ in (b) saturates at a lower field $H_s' \sim 3.6$ MA/m than 5.9 MA/m in (a).

in 10 nm Co-granules by heating in H_2 gas. A presumed value of $\sigma_s(s)$ as small as 143 Am^2/kg reveals an as thin GSP film as of a monatomic layer. Such a high $\sigma_s(s)$ in GSP is plausible in an enhanced magnetic moment μ_n of Co atoms in it on their partial surface oxidation. For example, $\mu_n = 1.75\ \mu_B$ for a free Co atom while 4.2 μ_B for a free Co^{2+} cation [27].

In a non-magnetized sample, the magnetic spins S_i and S_j in the two regions likely order in opposite directions in a low energy equilibrium spin-configuration, $\sum_{i<j} S_i.S_j = 0$. Application of a magnetic field H, to measure its $\sigma_s(t)$, excites them along it in their high-energy spin states. At a sufficiently enough value of H to attain the $\sigma_s(t)$, the spins in the two regions are set-up essentially in a single direction along the H, i.e., $\sigma_s(t) = \sigma_s(c) + \sigma_s(s)$. As can be inferred from the $\sigma(t)$ vs. H magnetization curve (Fig. 5a), the surface spins in GSP excite and align at relatively high H, extending the saturation of their magnetization $\sigma_s(t)$ to as high H as $H_s' \sim 5.9$ MA/m. The spins in the core, which impart a major part of $\sigma_s(t)$, magnetize rather easily at much lower fields $H_s' \leq 3.6$ MA/m (Fig. 5b) in the sample after cleaning up the GSP by heating it in H_2 gas.

As mentioned above, the increase in $\sigma_s(t)$ in small Co-granules over the bulk value indicates formation of more unpaired electrons n in the Co : $3d^{7+\delta}4s^{2-\delta}$ valence band. For FCC bulk cobalt, $\sigma_s(t) = 166.1$ Am^2/kg, which corresponds to $\mu_n = 1.75\ \mu_B$ magnetic moment per atom, gives an effective value of $n = 0.94$, or $\delta = 1.94$, according to the spin magnetic moment of the n electrons [27], i.e.

$$\mu_n = (g\mu_B/2)\sqrt{n(2n+1)} \qquad (4)$$

with $g = 2.17$ the Lande g-factor [27]. It ascribes a specific electronic structure of 8 paired and 0.94 unpaired electrons in the 3d band, leaving 0.06 electrons in the $4s^{2-\delta}$ conduction band. A similar electronic configuration with 0.06 holes in the 3d band, i.e. 5 spins up and 4.06 down, leaving 0.06 electrons in the conduction band, ascribes the same n or μ_n value, but it is not a feasible electronic structure of cobalt. It involves

a larger number of 9.06 valence electrons than a total of 9 ones available in it. In larger Co-granules of $D \sim 20$ nm, all the nine valence electrons occupy only the 3d band, with $n = 1$ unpaired d-electron, according to their observed $\sigma_s(t) = 178$ Am^2/kg or $1.88\mu_B$.

3.2.2. Surface-spin-glass (SSG) structure

The large IC region, with a large surface area Ω or interface energy $E_{IC} = \Omega\gamma_{IC}$ (with γ_{IC} the interface energy density), in Co-granules of an average 10 nm or smaller diameters configures a modified spin distribution of it than in the core, forming a biphasic magnetic (BPM) structure. The atoms in this presumably atomically thin region are reordered according to E_{IC} and the structure of the core so that its final structure has a minimal E_{IC} value. It does have a locally short range order structure of a droplet of a highly viscous liquid. It, therefore, presents a spin-glass like surface structure. At temperatures below a critical value T_F, in analogy to amorphous structure in a supercooled liquid, it can be regarded as to be frozen in a high magnetic viscosity state (metastable). This is exactly demonstrated by ZFC-FC (ZFC: zero field cooled and FC: field cooed) thermomagnetograms in Fig. 6.

The ZFC thermomagnetogram (Fig. 6a) is obtained by heating a sample of $D = 10$ nm granules (initially cooled in $H = 0$ field) between 4.2 and 380 K under a constant field $H = 1$ kA/m. It exhibits a peak in a typical blocking process of an assembly of superparamagnetic particles with a distribution of blocking temperatures at $T_B = 152$ K. In the classical theory of superparamagnetic particles [27], the T_B represents the critical temperature at which the metastable hysteretic response is lost for a particular experimental time frame. The hysteretic response is observed only over $T < T_B$ because thermal activation is not sufficient to allow the immediate alignment of spins with the applied field. Furthermore, the FC curve is measured during cooling the sample back to 4.2 K with the field. The $\sigma(t)$ in it monotonically increases as temperature decreases, deviating from the ZFC curve at T_F. Nevertheless, a close-up of the FC curve (Fig. 6c) at an expended scale of x-axis

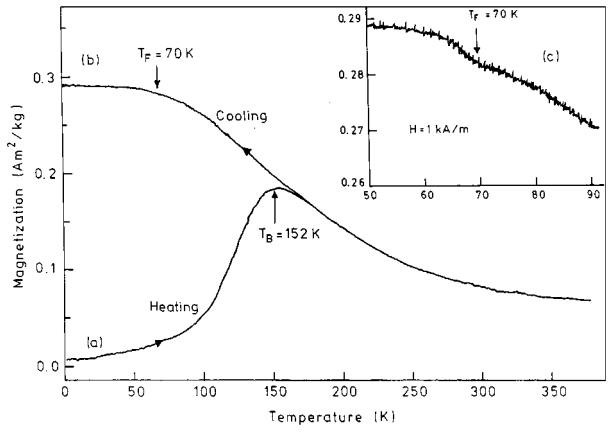

Figure 6 (a) ZFC and (b) FC (at $H = 1$ kA/m applied field) thermomagnetograms of Co-granules of diameter $D = 10$ nm. A peak appears in (a) at $T_B = 152$ K in their blocking process. (c) A close-up of (b) in the inset indicates a sudden increase in the magnetization at ~70 K.

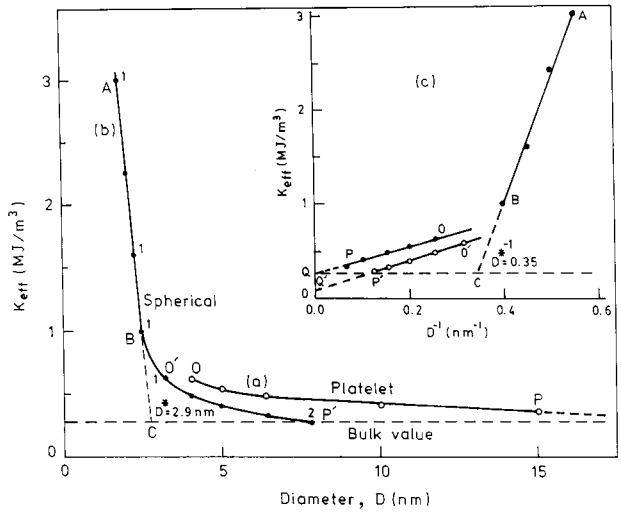

Figure 7 Anisotropy-energy constant K_{eff} as a function of average diameter D of Co-granules of (a) platelet and (b) spherical shapes. Extrapolation of its straight line part of AB to the bulk K_{eff} value at point C determines the critical $D^* = 2.9$ nm value of D, below which it has the linear D dependence. The figures in the inset are the linear plots of K_{eff} with D^{-1} according to relation (8). Points Q and Q′ are intersections of the experimental lines of OP and O′P′ to the K_{eff}-axis The data marked as (1) and (2) are taken from ref. [5, 14].

indicates a sudden increase in $\sigma(t)$ at $T_F \sim 70$ K, which ascribes the onset of the freezing process of the magnetic spins in the SSG layer. As $T \to T_F$, part of magnetic spins excited in high-energy thermal activation states relax and ultimately set-up aligned in the direction of H at T_F, and result in the increased $\sigma(t)$. The ferromagnetic (F) core changes its orientation by coherent rotation with a SSG layer that slowly relaxes in the H-direction according to its anisotropy energy K.

An average value of effective $K = K_{eff} \cong 0.42$ MJ/m^3 (Fig. 7a) is estimated using the observed $V = 150$ nm^3 and $T_B = 152$ K for $D = 10$ nm Co-granules (platelets) in the well-known relation [5, 27],

$$K_{eff} = \frac{30 K_B T_B}{V}, \tag{5}$$

with $K_B = 1.3807 \times 10^{-23}$ J/atom-K the Boltzmann's constant. Co-granules of a spherical shape, $D = 7.8$ nm [14], although have a similar $T_B = 160$ K, do not show a significant change in K_{eff} over the bulk value. A manifested value of K_{eff} in this case appears at much smaller D below 5 nm [5] (cf. Fig. 7b). A $K_{eff} = 2.25$ MJ/m^3 thus has been found at as small D as 2.0 nm, consistent with $K_{eff} = 3.0$ MJ/m^3 reported for spherical Co-granules of $D = 1.8$ nm [5]. As shown in Fig. 7, the K_{eff} involves two distinct D-dependence in this region of curve of OP in the platelet or the curve of ABO′P′ in the spherical morphology. The slope of the $K_{eff} - D$ curve changes prominently in the latter case at $D = D^* \cong 2.9$ nm. Here, D^* defines the critical value of D below which the value of K_{eff} is rapidly boosted up by the quantum-confined size effect of it. It is determined by extrapolation of the $K_{eff} - D$ straight line of AB to the bulk K_{eff} value at point C (Fig. 7b).

A peculiarly enhanced surface anisotropy determines the enhanced K_{eff} in so small granules. In this case, the

total anisotropy energy for a granule of volume V can be written as [23]

$$E_a = K_{eff}V = K_vV + K_sA. \quad (6)$$

On dividing by V it results in

$$K_{eff} = K_v + K_s(A/V), \quad (7)$$

where K_v and K_s are the volume and surface-energy constants. A spherical or cubid geometrical shape of diameter or side D has $A/V = 6/D$. A thin platelet of a large aspect ration D/δ, as in this example, gives a further larger A/V ratio. Thus in a more specific and realistic form Equation 7 can be expressed as

$$K_{eff} = K_v + \left[\frac{6\Phi}{D}\right]K_s, \quad (8)$$

where Φ defines deviation from its ideal value of unity in a perfect spherical or cubid shape.

According to Equation 8, a linear plot of K_{eff} with D^{-1}, in Fig. 7c, determines $K_v = 0.09 \pm 0.01$ MJ/m^3 and $K_s = 0.26 \pm 0.03$ mJ/m^2 in the spherical and $K_v = 0.27 \pm 0.01$ MJ/m^3 and $K_s = 0.23 \pm 0.03$ mJ/m^2 in the platelet morphology (assuming the same $\Phi \sim 1$ as in the spherical one) of Co-granules of $D > D^*$. The value of K_v estimated by the extrapolation of the straight line of OP to point Q with $D^{-1} \to 0$ for effectively large granules of platelet morphology is essentially the same as the bulk value. A spherical shape in so large granules is not feasible crystallographically. A similar extrapolation of K_{eff} to $D^{-1} \to 0$ in this case, therefore, results in an erroneously much smaller value of $K_v = 0.09 \pm 0.01$ MJ/m^3 by the intercept of the straight line of O′P′Q.

At D^{-1} above its critical value of $D^{*^{-1}} = 0.35$ nm^{-1}, a similar linear K_{eff} vs D^{-1} plot of ABC appears with an order of enhanced value of $K_s = 2.27 \pm 0.03$ mJ/m^3 (Fig. 7c). Its extrapolation to point C on the bulk K-line specifies the $D^{*^{-1}} = 0.35$ nm^{-1} value only above which it obeys the involved process of D-dependence of K_{eff}. In a more practical form this relation can be rewritten by shifting the origin of the co-ordinates from (0, 0) to $(D^{*^{-1}}, 0)$ so that the K_{eff} reads as K_v at $D^{-1} = D^{*^{-1}}$. The replacement of D^{-1} by $D^{-1} - D^{*^{-1}}$ according to it in Equation 8 and then a minor re-arrangement of the terms yields

$$K_{eff} = K_v + \frac{6\Phi}{DD^*}(D^* - D)K_s, = K_v + \frac{6\Phi}{D^*}\left[\frac{D^*}{D} - 1\right]K_s, \quad (9)$$

with $D \le D^*$. Obviously, in this relation, as $D \to D^*$, $K_{eff} \to K_v$, i.e. the bulk K-value. Now, if we define,

$$d = \left[\frac{1}{D^*}\left\{\frac{D^*}{D} - 1\right\}\right]^{-1} \quad (10)$$

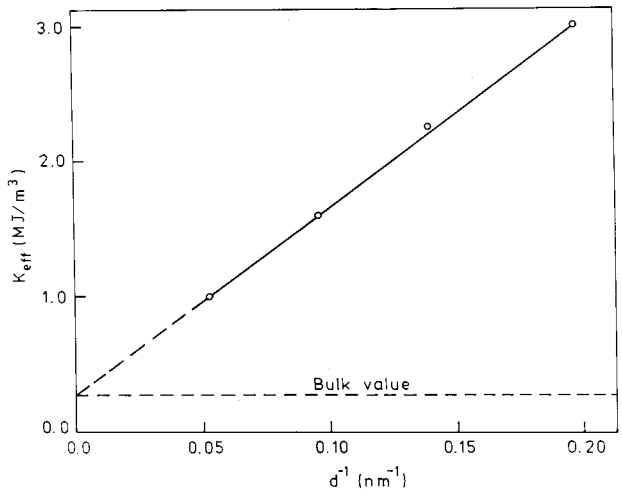

Figure 8 A linear plot of K_{eff} with reciprocal of reduced diameter d of the Co-granules according to Equation 11.

as the reduced value of D in Co-granules of confined size $D \le D^*$, then it simplifies Equation 9 as

$$K_{eff} = K_v + \left[\frac{6\Phi}{d}\right]K_s. \quad (11)$$

This is phenomenologically similar to Equation 8 discussed above. It is plotted in Fig. 8. As expected, it yields a more or less the same value of $K_s = 2.28 \pm 0.03$ mJ/m^2 as obtained by a direct K_{eff} vs D^{-1} plot according to Equation (8) within the experimental errors.

The value of $K_s = 2.28 \pm 0.03$ mJ/m^2 for Co-granules is as larger as ~30 times a value of 0.09 mJ/m^2 analyzed for similar spherical granules of α-Fe by their Mossbauer spectrum [23]. Also the value of $K_v = 0.27$ MJ/m^3 is roughly six times larger in cobalt [5, 27]. A dramatically improved $K_s = 1.0$ kJ/m^2 appears in α-Fe thin films of a submicrometer thickness [43]. Unfortunately, no other report is available on cobalt to perform a direct comparison of K_s obtained by an independent method. Nevertheless, altogether the results demonstrate, qualitatively, that the surface anisotropy is inherently related with the structure, morphology, and effective size of the sample. A small sample of quantum confined size of a largely modified original crystallographic shape of it by its large E_{IC} surface-energy thus exhibits a large value of its K_s.

In terms of the micromagnetic structure, in these small granules, in which 20 to 60% of the total atoms form the grain surface [18, 44], the total magnetic spins in IC becomes compatible to that in the core. A redistribution of the spins, if it is different in the two regions, occurs in this case, forming a sample of a more or less single spin distribution. It accords with its enhanced K value from 0.42 to 2.25 MJ/m^3 (Fig. 7) with an enhanced σ_s(t) from 173 to 216 Am^2/kg (or 2.28 μ_B per atom), in Fig. 9, in a decrease of its size D from 10 to 2.0 nm. Such a high σ_s(t) in Co : $3d^{7+\delta}4s^{2-\delta}$ can be ascribed using the mixing between the d and s-valence bands. For example, the average $\sigma_s(t) = 2.28$ μ_B magnetic moment observed per Co atom in 2.0 nm granules

TABLE II Observed magnetic moment μ_n, calculated spin and orbital magnetic moments, $3d^{7+\delta}4s^{2-\delta}$ band structure, and number of unpaired electron spins (n) in the 3d-band in the FCC Co-granules

Sample	μ_n (μ_B/atom)	$3d^{7-\delta}4s^{2-\delta}$ Band structure			Spin-orbit (S-O) coupling[a] (μ_B/atom)			S-O + Orbital polarization[a] (μ_B/atom)		
		$3d^{7+\delta}$	$4s^{2-\delta}$	n	Spin	Orbital	Total	Spin	Orbital	Total
Bulk										
	1.75	8.94	0.06	0.94	1.595	0.079	1.674	1.596	0.122	1.718
Granules										
$D = 20$ nm	1.88	9.00	0.00	1.00						
$D = 10$ nm	1.83	8.97	0.03	0.97						
$D = 2.0$ nm	2.28	8.75	0.25	1.25						

[a]These calculated values of the magnetic moments are reported from ref. 8.

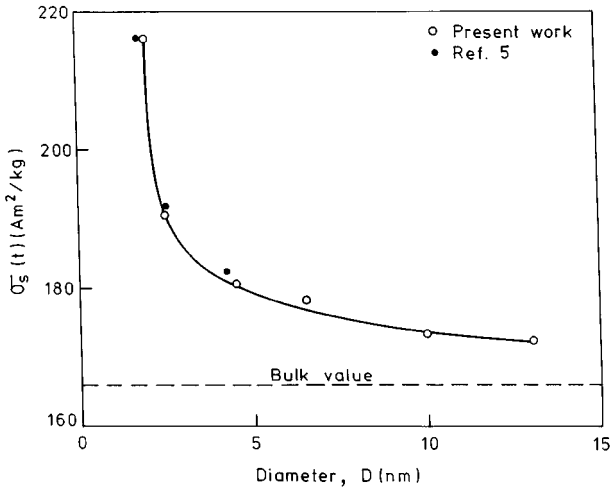

Figure 9 Saturation magnetization (σ_s) of Co-granules at 4.2 K (bulk $\sigma_s = 166.1$ Am^2/kg).

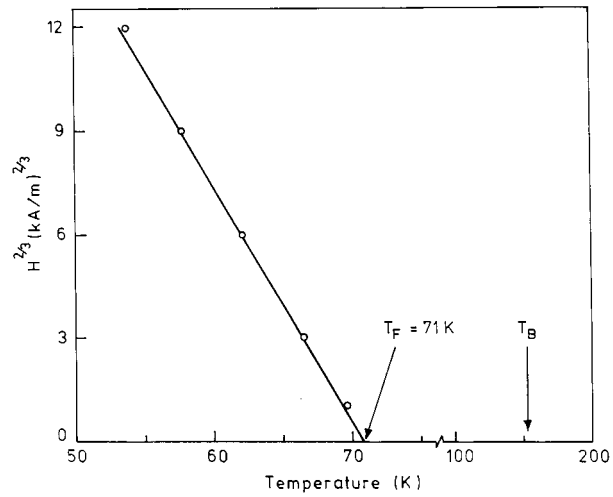

Figure 10 Magnetic field (H) dependence of the spin-glass transition temperature T_F showing the AT line, i.e. $\delta T_F \propto H^{2/3}$. $T_F(H=0) \simeq 71$ K is obtained by extrapolating the AT line back to $H = 0$.

gives an average $n = 1.25$ unpaired electrons in the d-band according to relation (4). As described above, it ascribes 1.25 holes in the d-band, i.e. 5 spins up and 3.95 spins down, leaving a total of 0.25 electrons in the conduction (4s) band. It might have a correlation with a small ~4.6% expansion of the lattice and/or atomic volume observed in small granules.

The spin-orbit (SO) coupling and SO and/or orbital polarization, which, in fact, are modified with the modified $3d^{7+\delta}4s^{2-\delta}$ band structure, are two other important parameters which modify the total σ_s(t) in small granules. Gasche *et al.* [8] calculated spin and orbital magnetic moments for FCC cobalt from self-consistent energy-band calculations. The result (cf. Table II) is that they have a very little 5 to 8% effect of these parameters. Their resultant value, 1.60 to 1.72 μ_B, of course, is far smaller than σ_s(t) = 2.28 μ_B observed per atom in $D = 2.0$ nm Co granules.

3.2.3. Dynamics of the SSG transition

The SSG transition temperature T_F at which the irreversible magnetization, defined as $\Delta\sigma = \sigma_{FC}(T) - \sigma_{ZFC}(T)$, differs from its zero value, demonstrating the onset of the freezing process of the magnetic spin in the SSG layer, decreases as H increases in the 0–42 kA/m range. At $H > 42$ kA/m, both ZFC and FC thermomagnetograms follow a common path with $\Delta\sigma = 0$. The variation of T_F with H follows the de Almeida-Thouless (AT) type power dependence [45], i.e.,

$$H_{AT}(T) = B\left[1 - \frac{T}{T_F}\right]^{3/2} + C \qquad (12)$$

where B and C are arbitrary constants. As plotted in Fig. 10, it represents a best fit to the experimental data points with a straight line. Its extrapolation to $H \to 0$ determines the absolute value of $T_F = 71$ K at $H = 0$.

This T_F transition appears a general feature of single magnetic domain particles of size $D \leq D_c$. We studied a variety of samples of pure metals [46], rare-earth (R) based RFe_2 or $R_2Fe_{14}B$ intermetallics [9, 47, 48], or ferrites [2, 11] and all of them have been found to have a T_F transition in the 0–300 K range [46]. Its position, shape and size is determined primarily by their size, morphology, surface structure, K_s and K_V anisotropies, and other experimental conditions.

Amongst all these examples, peculiarly in γ-Fe_2O_3, T_F persists to a relatively large field as 4.4 MA/m (few kA/m in others) [49]. A smaller field does not break up the strong coupling between the spins in the SSG layer as the origin of the high field irreversibility. STM (scanning tunneling microscopic) images of surfaces studied for stable iron oxides reveal a fascinating and complex surface topology of a biphase ordering of atomically

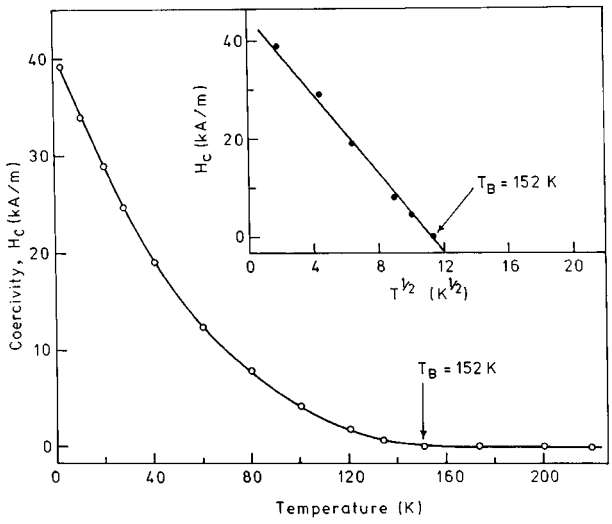

Figure 11 Temperature (T) dependence of coercivity H_c. The inset shows $H_c(T)$ to obey a linear $T^{1/2}$-dependence with a blocking temperature $T_B = 152$ K.

thin oxide surfaces [10, 50]. This is confirmed from their low energy electron diffraction (LEED) patterns [50]. Heijden *et al.* [10] reported that Fe_3O_4 magnetic layers separated by a thin nonmagnetic surface as of MgO of a nanometer thickness have a strong ferromagnetic coupling. The coupling strength increases dramatically with decreasing its thickness below 1.3 nm, confirming the existence of ferromagnetic bridges through the spacer.

A controlled partial surface oxidation of Co-granules in this example results in a similar biphase layered surface structure. An oxygen content of 1 to 2 at % has been analyzed in as small Co-granules as of $D = 10$ nm by elemental analysis. This is of current interest in the growth and properties of a short of mesoscopic magnetic structure, especially important as high-density storage media [12, 50]. Desirably modified magnetic properties with the ordered biphase magnetic structure in small granules are promising the development of novel magnetic materials and their devices.

3.2.4. Coercivity

The coercivity H_c, which is zero at $T \geq T_B$, monotonically increases with a decrease in temperature T below T_B, as portrayed in Fig. 11. It follows an empirical relation,

$$H_c(T) = H_c(0)\left[1 - \left\{\frac{T}{T_B}\right\}^n\right] + C \qquad (13)$$

at $T \leq T_B$, with the exponent $n \sim 1/2$ and the constant $C = 0$ for thin platelets of FCC cobalt of average diameter $D = 10$ nm and $T_B = 152$ K. The same relation was proposed by McHenry *et al.* [14] to describe temperature dependence of H_c in carbon coated Co granules of a spherical shape. For $T = 0$, it gives 0–K value of coercivity $H_c(0) = 40.0$ kA/m, in a close matching with an observed value of 39.8 kA/m at 4.2 K. The value of $n = 1/2$, which is most likely related to process of excitation/de-excitation of strongly co-related surface spins in SSG layer, is obtained by a numerical analysis of H_c at selected temperatures with relation (13). As shown in the inset to Fig. 11, it accords with a linear variation of H_C with $T^{1/2}$ at early $T \leq T_B$ temperatures.

The power increase of H_C over $T \leq T_B$ indicates a close relation of it with the freezing of the magnetic spins in the SSG layer in a preferred orientation at low temperatures, especially at $T \leq T_F$, which follows the T_B, with $\Delta T = T_B - T_F$ found to be 81 K. It can be attributed to the extra energy required for the switching of the magnetic spins that are pinned by the strong exchange interactions with the frozen SSG layer. The SSG layer surrounds the CC core which is single domain in nature. In a randomly oriented assembly of separated nanosized granules, it mediates as strong pinning barriers to the CC single domains. It inhibits local magnetic coupling between the granules in intimate contact, at low fields $H < H_c$, so that they behave to be ideal single domain magnetic particles with a locally pinned structure of magnetic spins at the interface with the SSG surface. Magnetically, the SSG layer is more hard to magnetization than the core as evident by its high field magnetization which saturates at a field as high as 5.9 MA/m (Fig. 5). In a strong ferromagnet, as in this case, in absence of the pinning barriers at grain boundaries, the domain walls run continuously from grain to grain without an interruption through several grains, forming an extended domain structure with a low H_c value [48, 51].

The $H_c = 39.5$ kA/m (at 4.2 K) observed for thin platelets is considerably smaller even than a value of $\sim$103.5 kA/m reported at RT for spherical shaped granules of similar size of FCC cobalt [1]. Chen *et al.* [5] studied H_c in spherical particles of much smaller diameters of 1.8 to 4.4 nm at selected temperatures between 2 and 300 K. A H_c as large as 91.5 kA/m (at 10 K) was found at D as small as 4.4 nm. This marked difference in H_c in the two morphologies can be ascribed by invoking in contributions of the H_s (surface) and H_b (shape) anisotropies. It can be formulated using Stoner-Wohlfarth theory [29], which predicts its value of

$$\begin{aligned} H_c(0) &= P\{H_a - H_s - H_b\} \\ &= P\{H_a - H_{sb}\}, \end{aligned} \qquad (14)$$

with

$$H_{sb} = H_s + H_b, \qquad (15)$$

for an assembly of non-interacting uniaxial single domain particles, where P is a geometrical parameter [52]. The P takes a value of 0.48 for thin platelets (single domain) with a large $D/\delta \geq 3$ aspect ratio [12, 52]. An average value of $H_{sb} \sim H_b$, with $H_s \sim 0$, successfully describes its contribution in H_c in hard magnetic particles [2, 29, 52] in which it is very small as compared to the $H_a = 2K_1/\sigma_s$ value, with K_1 the first anisotropy-energy constant. $H_b = 0$ for a perfect spherical and $4\pi\sigma_s$ for a thin platelet shape (in the direction of K_1 perpendicular to its flat surface). Other shapes have the values in between these two values.

For similar particles of a soft magnetic material, in which H_{sb} or $H_b \geq H_a$, a modified relation (14) can be used. According to our experimental results, it can be

TABLE III Saturation magnetization σ_s, coercivity H_c, and effective anisotropy-energy constant K_{eff} for small granules of FCC allotrope of pure cobalt metal obtained from the chemical-reduction of the metal cations

Structure	σ_s(Am^2/kg) RT	σ_s(Am^2/kg) 4.2 K	H_c (kA/m)[a]	K_{eff} (MJ/m^3)[a]
Amorphous	135	150	0.80	—
FCC structure				
(a) Bulk	164.8[b]	166.1[b]	—	0.27[c,d]
(b) Nanocrystalline				
$D =$ 10 nm	161.0	173.0	39.8	—
$D =$ 20 nm	165.0	178.0	35.0	—
$D =$ 1.8 nm	$\leq$40[c]	216[c]	0	3.0[c]
HCP structure (Single crystal)	161.8[b]	163.1[b]	0	0.53[d]

[a]The values for the H_c or K_{eff} are reported at 4.2 K.
[b, c] and [d] These values are taken from references 41, 5, and 27, respectively.

written as

$$H_c(0) = P H_a\left[1 - \left\{\frac{H_{sb}}{H_a}\right\}A\right]. \qquad (16)$$

Here, the function $f(H_{sb}) = (H_{sb}/H_a)A$ in the second term defines an effective structural fractional value of H_{sb} which imparts the total H_c. The coefficient A has a positive value between 0 and 1 so that it defines a positive fractional $f(H_{sb}) \leq 1$ value. In the case of a hard magnetic material, in which H_b/H_a ratio is already smaller than 1, this relation applies with $A = 1$. With the standard $H_a = 588.9$ kA/m value (as for the HCP cobalt) [27], it gives an optimal value of $H_c(0) = 282.7$ kA/m for spherical particles ($H_b = 0$), with the same value of $P = 0.48$ as for the platelets [12, 52]. That is still as lager as twice the experimental value. In fact, the particles in question have some magnetostatic interactions, which further lowers its final value as follows;

$$H_c(p) = H_c(0) - \alpha\beta\sigma_s \qquad (17)$$

where α is the packing fraction and the coefficient $\beta = 1.7/4\pi$ for randomly packed particles [53]. It yields $H_c(p) =$ 120.9 kA/m, with the experimental parameters $\alpha = 0.82$ and $\sigma_s = 165$ Am^2/kg (cf. Table III), consistent with an optimal 119.4 kA/m value reported by Gong *et al*. on single domain, $D_c = 20$ nm, Co granules of a spherical shape [1].

For the morphology of a thin Co platelet, $D = 10$ nm, with shape anisotropy $H_{sb} = 4p\sigma_s$, the same parameters with an empirical value of $f(H_{sb}) \sim 0.1$, i.e. $A \sim 0.1$, result in a decreased value of $H_c(P) \sim 40.8$ kA/m which accords with the observed 39.8 kA/m value (at 4.2 K). Whatever the basis of the selection of A, the result envisages that it sensitively modifies the final H_c if the morphology differs a perfect spherical shape. Its knowledge is important for designing of high H_{sb} single domain particles of an extremely small H_c, especially useful for magnetic switching applications [12, 13, 48].

4. Conclusions

A chemical co-reduction of dispersed Co^{2+} cations in a liquid results in separated granules of pure cobalt metal of a new FCC crystal structure of a controlled size of a nanometer scale. A proper adjustment of their concentration and pH permits a desired control of size and morphology of the granules. Small granules of an average diameter D below 5 nm assume a spherical shape. A platelet shape appears at bigger sizes. The FCC structure with a quantum confined size in small granules is peculiarly thermally stable over a wide range of temperature, 4.2–1023 K. A conventional bulk sample of pure cobalt metal obtained by other methods has a HCP structure and that undergoes a reversible HCP $\Leftrightarrow$ FCC martensite phase transformation at $\sim$700 K with a change of enthalpy $\Delta H = 440$ kJ/mol or volume $\Delta V/V \sim 0.36\%$ [30, 32]. According to the thermodynamics, the small granules assume a modified morphology and/or a modified crystal structure so that their total surface-energy Ω is minimum [46]. The Co-granules, $D \leq 20$ nm, in this example support the FCC structure as it involves an effectively smaller Ω than the HCP structure. That determines a lower value of enthalpy of its formation over the HCP structure. Therefore, it is substantially stable and does not transform to the HCP structure which is the most stable allotrope of cobalt otherwise.

The atoms in the grain-surface forms a spin-glass like metastable magnetic structure with a high configurational entropy of the core according to the basic principles of the thermodynamics. As expected, the atoms in the surface-spin-glass (SSG) have a presumably lower co-ordination number in a reduced symmetry of the core atoms. This results in a modified electronic structure of the $Co: 3d^{7+\delta}4s^{2-\delta}$ valance band, which involves a more number of unpaired $3d^{7-\delta}$ electrons than that in a core atom. As a matter of fact, a surface atom assumes a larger value of the spin-magnetic moment than a core atom. The magnetic spins in the SSG layer are ferromagnetically coupled to those in the core. The coupling strength increases drastically with increasing surface area in small granules, $D \leq 20$ nm, and is ascribed to the existence of ferromagnetic bridges through the interface. It successfully explains their enhanced value of saturation magnetization σ_s(t), by as much as $\sim$34%, observed over the bulk value. The effective anisotropy energy constant K_{eff} is monotonically increased by a more than an order of magnitude with a decrease in

D from 10 nm to 2.0 nm. A chemisorption of oxygen atoms at the grain-surface form a similar surface layer of partially oxidized Co atoms with a ferromagnetic coupling to the spins in the core.

The SSG undergoes a magnetic transition to a spin-frozen metastable magnetic state at a critical temperature $T_F = 71$ K. The T_F evolves following the well-known de Almeida-Thouless line [45], $\delta T_F \propto H^{2/3}$, for $H \leq 42$ kA/m. The thermomagnetograms in ZFC-FC (zero field cooled-field cooled) processes show an irreversibility below the blocking temperature T_B, which is found to be larger than T_F. At $T \leq T_B$, the SSG supports a high value of coercivity, $H_c(T)$, which monotonically increases with decreasing the temperature T, following a unique temperature dependence, $H_c(T) = H_c(0)[1 - T/T_B]^n$, with $n = 1/2$ and $H_c(0) = 40.0$ kA/m. The studies of the magnetization σ and anisotropy constant K_{eff} as a function of temperature (4.2–380 K) and/or the grain size (2–20 nm) demonstrate that these have a strong correlation with the density of the surface spins (DSS) and their dynamics. A large DSS in small granules determines an enhanced surface-anisotropy-energy (SAE). An average value of the SAE constraint $K_s = 2.28 \pm 0.03$ mJ/m^2 is determined by a linear plot of K_{eff} against D^{-1}, at $D \leq 2.9$ nm. The larger granules have an order of smaller magnitude of K_s.

Acknowledgement

The author is grateful to professor H. J. Fecht (of Faculty of Engineering, Ulm University, Germany) for fruitful discussion and for the use of his laboratory facilitates. This work is partially supported by the Alexander Humboldt Foundation, Germany, and by the Council of Scientific & Industrial Research, India.

References

1. W. GONG, H. LI, Z. ZHAO and J. CHEN, *J. Appl. Phys.* **69** (1991) 5119.
2. S. RAM and J. C. JOUBERT, *Phys. Rev.* **B44** (1991) (6825).
3. S. GANGOPADHYAY, G. HADJIPANAYIS, B. DALE, C. M. SORENSEN, K. J. KLABUNDE, V. PAPAEFTHYMIOU and A. KOSTIKAS, *ibid.* **B45** (1992) 9778.
4. S. RAM, *ibid.* **B49** (1994) 9632.
5. J. P. CHEN. C. M. SORENSEN, K. J. KLABUNDE and G. C. HADJIPANAYIS, *ibid.* **B51** (1995) 11527.
6. S. RAM, M. FEBRI, H. J. FECHT and J. C. JOUBERT, *Nanostruct. Mater.* **6** (1995) 473.
7. W. WEBER, C. H. BACK, A. BISCHOF, CH. WURSCH and R. ALLENSPACH, *Phys. Rev. Lett.* **76** (1996) 1940.
8. T. GASCHE, M. S. S. BROOKS and B. JOHANSSON, *Phys. Rev.* **B53** (1996) 296.
9. S. RAM, H. J. FECHT, S. HALDAR, P. RAMACHANDRARAO and H. D. BANERJEE, *ibid.* **B56** (1997) 726.
10. P. A. A. VAN DER HEIJDEN, P. J. H. BLOEMEN, J. M. METSELAAR, R. M. WOLF, J. M. GAINES, J. T. W. M. VAN DER EEMEREN, P. J. VAN DER ZANG and W. J. M. DE JONGE, *ibid.* **B55** (1997) 11569.
11. S. RAM and J. C. JOUBERT, *IEEE. Trans. Magn.* **MAG-28** (1992) 15.
12. S. RAM. *J. Magn. Magn. Mater* **82** (1989) 129.
13. M. P. SHARROCK, *IEEE. Trans. Magn.* **MAG-25** (1989) 4374.
14. M. E. MCHENRY, S. A. MAJETICH, J. O. ARTMAN, M. DEGRAEF and S. W. STALEY, *Phys. Rev.* **B49** (1994) 11358.
15. K. RAJ and R. MOSKOWITZ, *J. Magn. Magn. Mater.* **85** (1990) 233.
16. M. CHANDRAMOULI, A. HUTTEN and G. THOMAS, *Scripta Met. Mater.* **30** (1994) 671.
17. H. GLEITER, *Prog. Mater. Sci.* **89** (1989) 223.
18. R. W. SIEGEL, *Ann. Rev. Mater. Sci.* **21** (1991) 559.
19. L. I. CANHAM, *Appl. Phys.* **57** (1990) 1046.
20. C. KITTEL, *Phys. Rev.* **70** (1946) 965.
21. M. LEDERMAN, S. SCULTZ and M. OZAKI, *Phys. Rev. Lett.* **73** (1994) 1986.
22. M. ALDEN, S. MIRBT, H. L. SKRIVER, N. M. ROSENGAARD and B. JOHANSSON, *Phys. Rev.* **B46** (1992) 6303.
23. F. BØDKER, S. MØRUP and S. LINDEROTH, *Phys. Rev. Lett.* **72** (1994) 282.
24. W. DE HEER, P. MILANI and A. CHALETAIN, *ibid.* **65** (1990) 488.
25. A. J. COX, J. G. LOUDERBACK and L. A. BLOOMFIELD, *ibid.* **71** (1993) 923.
26. I. M. BILLAS, A. CHALETAIN and W. DE HEER, *Science* **265** (1994) 1682.
27. D. J. CHAIK and R. S. TEBBLE, Magnetic Materials (John Wiley & Sons, London, 1969).
28. L. NEEL, *Ann. Geophys.* **5** (1949) 99.
29. E. STONER and E.P. WOHLFARTH, *Philos. Trans. R. Soc. London* **A240** (1948) 599.
30. J. Y. HUANG , Y. K. WU and H. Q. YE, *Acta Mater.* **44** (1996) 1201.
31. W. WERNSDORFER, K. HASSELBACH, A. SULPICE, A. BENOIT, J. E. WEGROWE, L. THOMAS, B. BARBARA and D. MAILLY, *Phys. Rev.* **B53** (1996) 4341.
32. M. ERBUDAK, E. WETLI, M. HOCHSTRASSER, D. PESCIA and D. D. VVEDENSKY, *Phys. Rev. Lett.* **79** (1997) 1893.
33. O. KOBAYASHI, T. AIZAWA and J. KIHARA, *Mater. Trans. JIM* **9** (1996) 1497.
34. S. TRAPP, C. T. LIMBACH, U. GONSER, S. J. CAMPBELL and H. GLEITER, *Phys. Rev. Lett.* **75** (1995) 3760.
35. L. C. CHEN and F. SPAEPEN, *Nature* **336** (1988) 366.
36. S. RAM and G. P. JOHARI, *Philos. Mag.* **B61** (1990) 299.
37. S. RAM, *Phys. Rev.* **B42** (1990) 9582.
38. E. KLUGMANN, H. J. BLYTHE and F. WALZ, *Phys. Stat. Solidi (a)* **146** (1994) 803.
39. JCPDS Files 15.806 and 5.0727.
40. J. I. LANGFORD, *J. Appl. Crystallogr.* **11** (1978) 10.
41. L. J. SWARTZENDRUBER, *J. Magn. Magn. Mater.* **100** (1986) 573.
42. J. R. CHILDRESS and C. L. CHIEN, *Phys. Rev.* **B43** (1991) 8089.
43. K. B. URQUHART, B. HEINRICH, J. F. COCHRAN, A. S. ARROTT and K. MYRTLE, *J. Appl. Phys.* **64** (1988) 5334.
44. E. A. STERN, R. W. SIEGEL, M. NEWVILLE, P. G. SANDERS and D. HASKEL, *Phys. Rev. Lett.* **75** (1995) 3874.
45. DE ALMEIDA and D. J. THOULESS, *J. Phys.* **A11** (1978) 983.
46. S. RAM (Unpublished results).
47. S. RAM and J. C. JOUBERT, (a) *J. Appl. Phys.* **72** (1992) 1164 and (b) *Appl. Phys. Lett.* **61** (1992) 613.
48. S. RAM, *J. Mater. Sci.* **32** (1997) 4133.
49. B. MARTINEZ, X. OBRADORS, L. BALCELLS, A. ROUANET and C. MONTY, *Phys. Rev. Lett.* **80** (1998) 181.
50. N. G. CONDON, E. M. LEIBSLE, A. R. LENNIE, P. W. MURRAY, D. J. VAUGHAN and G. THOMTON, *ibid.* **75** (1995) 1961.
51. F. E. PINKERTON and C. D. FUERST, *J. Magn. Magn. Mater.* **89** (1990) 139.
52. B. T. SHIRK and W. R. BUESSEM, *J. Appl. Phys.* **40** (1969) 1294; *J. Amer. Ceram Soc.* **53** (1970) 192.
53. D. F. ELDRIDGE, *J. Appl. Phys.* **32** (1961) 2478.

Received 22 April
and accepted 13 December 1999